

1

Coastal and regional marine heatwaves and cold-spells in the Northeast Atlantic

Amélie Simon^{1*}, Coline Poppeschi², Sandra Plecha¹,
Guillaume Charria², Ana Russo¹

¹ Universidade de Lisboa, Faculdade de Ciências, Instituto Dom Luiz (IDL), 1749-016, Lisboa, Portugal

² Ifremer, Univ. Brest, CNRS, IRD, Laboratory for Ocean Physics and Satellite remote sensing (LOPS), IUEM, 29280 Brest, France

*corresponding author: Dr. Amélie Simon; ajsimon@fc.ul.pt

Abstract

The latest IPCC report describes an increase in the number and intensity of marine heatwaves (MHWs) and a decrease in marine cold-spells (MCSs) in the global ocean. However, these reported changes are not uniform on a regional to local basis and it remains unknown if coastal areas follow the open ocean trends. Ocean temperature measurements collected by satellites (from 1982-2022) and 13 coastal buoys (from 1990-2022) are analyzed in the Northeast Atlantic and three subregions: English Channel, Bay of Brest and Bay of Biscay. The activity metric, combining the number of events, intensity, duration and spatial extent, is used to evaluate the magnitude of these extreme events. The results from *in situ* and satellite datasets for each of the studied regions are quite in agreement, although the satellite dataset underestimates the amplitude of activity for both MHWs and MCS. This supports the applicability of the method to both *in situ* and satellite data, albeit with caution on the amplitude of these events. Also, this localized study in European coastal Northeast Atlantic water highlights that similar changes are being seen in coastal and open oceans regarding extreme events of temperature, with MHWs being more frequent, longer, and extending over larger areas, while the opposite is seen for MCSs. These trends can be explained by changes in both the mean and variance of sea-surface temperature. Besides, the pace of evolution and dynamics of marine extreme events differs among the subregions. Among the three studied subregions, the English Channel is the region experiencing the strongest increase in summer MHWs activity over the last four decades. Summer MHWs were very active in the English Channel in 2022 due to long events, in the Bay of Biscay in 2018 due to intense events and in the Bay of Brest in 2017 due to a high occurrence of events. Winter MCSs were the largest in 1987 and 1986 due to long and intense events in the English Channel. Finally, our findings suggest that at an interannual time scale, the positive North Atlantic Oscillation favors the generation of strong summer MHWs in the Northeast Atlantic, while dominant low-pressure conditions over Northern Europe and a high off the Iberian Peninsula in winter dominates for MCSs. A preliminary analysis of air-sea heat flux suggests that, in this region, low cloud coverage is a key parameter for the generation of summer MHWs while strong winds and high cloud coverage is important for the apparition of winter MCSs.

44
45
46
47
48
49
50

51 **Keywords**

52
53 Extreme events, Sea Surface Temperature, Long-term *in situ* observations, Satellite data,
54 Marine heatwaves, Marine cold-spells, Bay of Biscay, English Channel, North Atlantic
55 Oscillation

56
57
58
59

60 **1. Introduction**

61

62 Heatwaves and cold-spells are extreme events in which there is a strong anomaly in
63 temperature for a certain period which can occur at a regional spatial scale. This type of
64 phenomenon can occur both in the atmosphere and in the ocean, with remarkable
65 consequences both for terrestrial and marine ecosystems (Ruthrof et al., 2018). In the case of
66 marine events (hereafter referred to as marine heatwaves (MHWs) or marine cold-spells
67 (MCSs)), severe large-scale biodiversity losses may occur such as species extinction, habitat
68 destruction and abrupt changes in the geographical distribution and structure of communities,
69 as well as the nutrient cycle (Frölicher and Laufkötter, 2018; Ruthrof et al., 2018; Smale et al.,
70 2019). Additionally, a decrease in the density of marine algae forests and coral bleaching
71 (Wernberg et al., 2016; Smale et al., 2019) have also been reported.

72 The frequency, duration and intensity of these extreme phenomena affecting ocean
73 systems have been increasing worryingly in recent decades (Lima and Wetthey, 2012; Oliver
74 et al., 2018; Frölicher et al., 2018; Plecha and Soares, 2020; Simon et al., 2022 and many
75 others). As a result of global and regional warming heavily influenced by anthropogenic
76 factors, the intensity and annual number of MHWs will continue to accelerate globally (Oliver
77 et al., 2019; Plecha et al., 2021). Conversely, as oceans warm, MCSs are diminishing
78 (Schlegel et al., 2021; Simon et al., 2022) and are expected to continue fading in future
79 climate conditions (Yao et al., 2022). However, these evolutions are not uniform regionally
80 and it remains unknown if coastal areas follow the open-ocean trends.

81 This paper focuses on the coastal and regional Northeast Atlantic and three subregions
82 (English Channel, Bay of Brest and Bay of Biscay) as these zones are important for socio-
83 economic activities (e.g. fishery; Guo et al., 2022) and have contrasted dynamical
84 environment. Plecha et al. (2021) studied MHWs annual features in the whole North Atlantic
85 using low-resolution satellite data at $1^\circ \times 1^\circ$ over the period 1971-2000. They show that in the
86 Bay of Biscay, the mean frequency is about 12 events per year and is characterized by ~ 12
87 days of mean duration and 0.4°C of mean intensity. Marin et al. (2021) did a global analysis
88 of MHWs in coastal areas over the period 1992–2016 based on a satellite multi-product at a
89 resolution from 0.25×0.25 up to 0.05×0.05 . They found that in the Bay of Biscay and
90 English Channel from 1992–2016, MHWs occurred on average 3 times per year lasting about
91 20 days with a mean intensity of 1.5°C . Here we focus on these regions on the seasonal
92 features, such as summer MHWs and winter MCSs with a satellite product at 0.25×0.25 .

93

94 Long-term ocean warming is an important driver of the increase of MHWs (Frölicher
95 et al., 2018) and the diminishing of MCSs (Schlegel et al., 2021; Wang et al., 2022) but does
96 not explain shorter variabilities of these events, or justify their interannual variability. These
97 marine extreme events are also driven by other local and remote processes acting across a

98 large range of spatial and temporal scales (Holbrook et al., 2019; Schlegel et al., 2021).
99 Modes of atmospheric circulation variability can induce anomalous sea surface temperature
100 (SST) through modification of air-sea heat fluxes and/or displacement due to ocean current
101 advection (Deser et al., 2010) which for extreme cases, can lead to MHWs or MCS.

102 Interannual summer atmospheric variability in the North Atlantic-European sector has
103 been shown to be predominantly led by the summer North Atlantic Oscillation (SNAO)
104 pattern. The SNAO is identified as strong high-pressure anomalies dominating Northern
105 Europe and weaker low-pressure over Greenland and the Iberian Peninsula which explains
106 about 20% of the variance using sea-level pressure (Hurrell et al., 2003). The SNAO is
107 recognized as a more northerly location and smaller spatial scale than the winter NAO pattern.
108 During the positive phase of the SNAO, Northern Europe experiences drier, warmer and
109 reduced cloudiness conditions, and the Bay of Biscay, the English Channel, and the North and
110 Baltic Seas undergo warmer SST (Folland et al., 2009). The East Atlantic (EA) pattern is also
111 identified as a dominant mode of North Atlantic atmospheric variability (Barnston and
112 Livezey, 1987), which is particularly important for the northwest Iberian Peninsula climate in
113 all seasons (Lorenzo et al., 2008). It is a North–South dipole that spans the entire North
114 Atlantic Ocean, with centers southeastward to the NAO pattern (winter and summer).

115 Although there is strong evidence of the influence of large-scale features, no
116 consensus exists on atmospheric patterns associated with summer MHWs in the Bay of
117 Biscay and the English Channel. On one side, Holbrook et al. (2019) identify the Bay of
118 Biscay as a region for which there is a significant increase in annual MHWs days during a
119 positive phase of the NAO, based on a linearly detrended SST with satellite data and NAO
120 index. On the other side, Izquierdo et al. (2022a) suggest, based on the analysis of two *in situ*
121 buoys in the coastal south of the Bay of Biscay, that the incidence, duration, and intensity of
122 spring-summer MHWs is higher during the positive phase of the EA. However, for each of
123 these two studies, only one climate index out of the numerous modes of summer atmospheric
124 variability in the North Atlantic-Europe sector was considered.

125 MCSs have also been reported to occur as a response to atmospheric forcing through
126 anomalous winds and air-sea heat fluxes, especially in coastal regions where cold air
127 outbreaks over shallow water can cause rapid chilling of water (Crisp, 1964; Schlegel et al.,
128 2021). But to the best of our knowledge, no study has been published focusing on the
129 connection between MCSs and atmospheric circulation in the Bay of Biscay and the English
130 Channel.

131
132 At a more regional scale, Guinaldo et al. (2023) linked the 2022 MHW off France to
133 above-average solar radiation, below-average cloud coverage and negative wind speed
134 anomalies showing also the importance of hydrodynamic conditions such as the tide that
135 allows turbulent vertical mixing. This explains why the Mediterranean sea with weak tidal
136 ranges presents a more pronounced response to MHWs (Darmaraki et al., 2019; Simon et al.,
137 2022). Other studies have been carried out in terms of processes and detection of MHWs in
138 the Bay of Biscay but only along the Spanish Cantabrian coast. Namely, Izquierdo et al.
139 (2022b), found a steady increase in SST from 1998 to 2019, which was reflected in MHWs
140 occurrence and consequent match-up to report population shifts in coastal macroalgae. In a
141 second study, Izquierdo et al. (2022a) compared MHWs with satellite data and found a 6-fold
142 increase in their incidences in the last four decades with half of this increase related to climate
143 change.

144 Several studies focus on the impact of MHWs or MCSs on biological systems,
145 covering the areas of the Bay of Biscay, the English Channel or the Spanish Cantabrian coast,
146 reaching as far back as the 60s of the XXth century. These studies analyzed the atmospheric
147 cold-spells of the winter of 1962-1963 on the English coast and the impact on marine animal

148 mortality such as *Pecten Maximus* (Crisp, 1964) or migration of species such as flounder
149 (Sims et al., 2004). In the English Channel, Gomez and Souissi (2008) made the link between
150 the MCS of 2005 and the absence of the spring bloom of *Phaeocystis*. A delay in the initiation
151 of the phytoplankton bloom caused by the presence of MCS at the end of winter in the Bay of
152 Brest and in the Bay of Vilaine (in the Northern part of the Bay of Biscay) is observed by
153 Poppeschi et al. (2022). The impact of MHWs on biology is even more studied than the cold
154 counterpart. Gomez and Souissi (2008) show the link between the heatwave of 2003 in the
155 English Channel and the abundance of dinoflagellates. Joint and Smale (2017) demonstrate a
156 link between MHWs and microbial activity assemblage in the English Channel which controls
157 biogeochemical cycles in the ocean. The MHW of 2018 in the English Channel is present in
158 the literature for its mortality mass impact on mussels (Seuront et al., 2019), its link to fucoids
159 (Mieszkowska et al., 2020) or harmful phytoplankton blooms (Brown et al., 2022).
160 Predictions at the atmospheric scale point to an increase in the future of heatwaves in the Bay
161 of Biscay (Chust et al., 2011) and a decrease in marine fauna (Wetthey and Woodin, 2022).

162

163 In this context, we aim to describe and explain the evolutions of the MHWs over
164 summer and MCSs over winter activity in the Northeast Atlantic and to investigate the
165 regional variability in three subregions: the English Channel, the Bay of Brest and the Bay of
166 Biscay. The analysis will rely on both *in situ* and satellite data to address MHWs and MCSs
167 activity, aiming to evaluate the impact of such events in coastal regions and in the open ocean.
168 This approach will allow us to evaluate the potential use of *in situ* measurements to detect,
169 characterize and understand such extreme events. In the last section of this paper, we focus on
170 the influence of the interannual atmospheric mode of variability involved in the occurrence of
171 MHWs and MCSs in the Northeast Atlantic by finding the atmospheric circulation occurring
172 in phase with most of the strongest events.

173

174

175 2. Material and methods

176

177 2.1 Satellite and reanalysis data

178

179 The global SST data used in this study results from a combination of different
180 observational platforms, including satellites, ships, buoys and Argo floats, provided by the
181 National Oceanic and Atmospheric Administration (hereafter OISST; Reynolds et al., 2007;
182 Huang et al., 2020). The satellite products have a daily temporal coverage for the 1982-2022
183 period and are interpolated to a regular global grid of $1/4^\circ$ spatial resolution. Monthly
184 geopotential height at 500 hPa (Z500), surface net short-wave radiation flux, surface net long-
185 wave radiation flux, surface sensible heat flux and latent radiation heat flux data were
186 obtained from the European Center for Medium-Range Weather Forecasts (ECMWF)
187 reanalysis data ERA5 at a spatial resolution of $0.25^\circ \times 0.25^\circ$ (Hersbach et al., 2019).

188

189

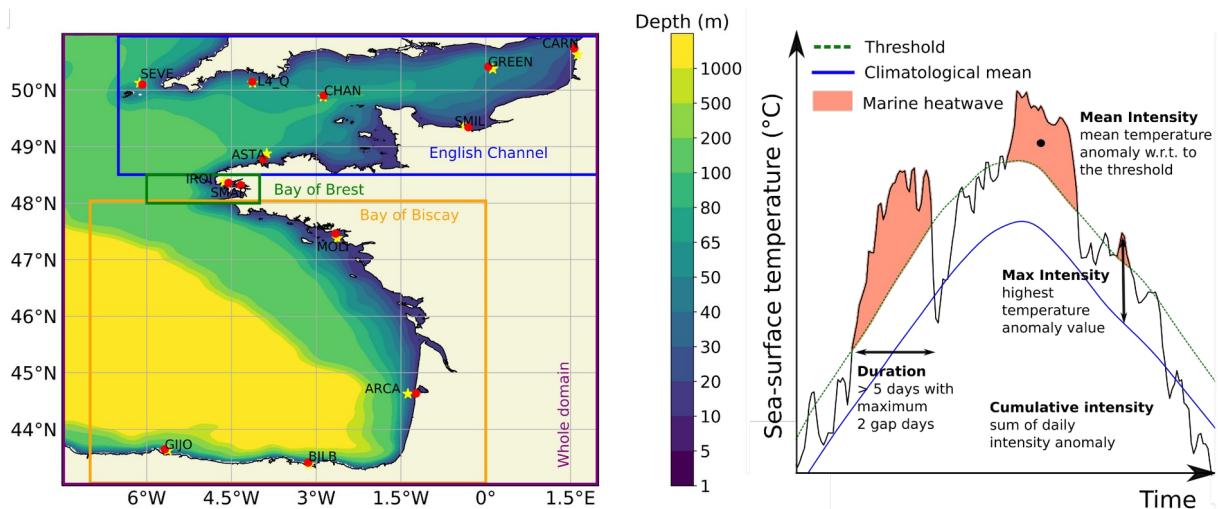
190 2.2 Buoy data

191

192 The *in situ* SST data are from autonomous coastal buoys that take continuous high-
193 frequency measurements from 10 minutes to 1 hour (Figure 1, left panel). These buoys are
194 from different European organizations, detailed below and in Table S1, covering the coastal
195 areas of the English Channel, the Bay of Brest and the Bay of Biscay.

196 The National Observation Infrastructure network (COAST-HF, www.coast-hf.fr)
197 operates 14 buoys taking measurements of several physical and biogeochemical data all

198 around French coasts. Among them, 7 buoys are used here and are located in the English
 199 Channel - CARNot (<https://doi.org/10.17882/39754>), SMILe (<https://doi.org/10.17882/53689>)
 200 and ASTAn; in the Bay of Brest - IROise (<https://doi.org/10.17882/74004>) and SMART
 201 (<https://doi.org/10.17882/86020>) and in the Bay of Biscay - MOLIt
 202 (<https://doi.org/10.17882/46529>) and ARCAchon. The Met Office (www.metoffice.gov.uk)
 203 manages several buoys in each facade of England and also at offshore sites. The buoys used
 204 here are located in the English Channel, on the South coast of England, SEVEN Stones;
 205 CHANnel and GREENwich. The Western Channel Observatory (WCO,
 206 www.westernchannelobservatory.org.uk), situated within the western English Channel
 207 operates two oceanographic moorings. The station L4_Q located near the city of Plymouth,
 208 approximately 7 km offshore is used here. Puertos del Estado (www.puertos.es) operated two
 209 buoys along the Spanish coast: BILBao and GIJOn located in the Cantabrian Sea, both of
 210 them are used here.
 211



212
 213 Figure 1: (Left) Map of the study area including the whole domain/Northeast Atlantic (purple
 214 box) as well as the three subregions which are the English Channel (blue box), the Bay of
 215 Brest (green box) and the Bay of Biscay (orange box). The buoys are represented by red dots
 216 and the closest satellite points are represented by yellow stars. (Right) Schematic of MHW
 217 detection and properties as defined by Hobday et al. (2016).
 218
 219

220 2.3 Detection of MHWs and MCS

221

222 To detect marine temperature extreme anomalies, we use the definition of Hobday et
 223 al. (2016). First, a climatology over 40 years, from 1982 to 2022, is calculated from the
 224 satellite product. Then, we apply the 90th percentile on summers (JJAS) for MHW and the 10th
 225 on winters (DJFM) for MCS. Finally, a MHW (MCS) is detected if values are above (below)
 226 the threshold for at least 5 days. For *in situ* data, the same detection method is applied
 227 considering the climatology calculated from the satellite product. Only seasons (summer or
 228 winter) with more than 80% of available data are analyzed.

229 To characterize MHW and MCS, we analyze parameters such as the number of events,
 230 the duration, the spatial extent and the cumulative intensity, defined as in Hobday et al. (2016)
 231 (Figure 1, right panel). We also explore an integrated indicator of these different parameters
 232 characterizing the marine temperature extreme events (MHWs and MCS), called activity and
 233 defined by Simon et al. (2022). This indicator estimates for each grid point the cumulative
 234 combination of the mean intensity, the duration and the affected area of each extreme event

235 within a selective time range (for example JJAS). This activity index accounts explicitly for
 236 the area, as in most SST products a grid cell area differs from one latitude to another and
 237 marine thermal events can expand over large areas. The activity is calculated for each grid
 238 point. It sums the product of the mean intensity, duration within the selected time range, and
 239 area of each detected event occurring within the selected time range. The activity is written as
 240 follows:

$$241 \quad Activity = \sum_{EE \in Time\ Range} mean\ intensity_{EE} \cdot duration_{EE \cap Time\ Range} \cdot area_{EE}$$

242
 243 Where $EE \in time\ range$, denotes the extreme event (EE) that occurs within the selected time
 244 range; the mean intensity of EE (in °C) is the mean temperature anomaly with respect to the
 245 threshold of the event; duration $EE \cap time\ range$ (in days) is the duration of the event that
 246 remains within the considered time range, and $area_{EE}$ (in km²) is the area affected by the
 247 discrete event within a predefined domain. Time series involving the activity metric for a
 248 domain are calculated as the mean of every grid cell considered. The activity for each station
 249 is computed in °C.days without considering the area influenced by the events as it can not be
 250 estimated from single localized stations.

251 This method of detection and characterization of marine thermal extreme events is
 252 performed over the whole domain of this study, referred to as the Northeast Atlantic (8° W to
 253 2° E - 43° N to 51° N) and at each station where *in situ* observations are available. As
 254 illustrated in Figure 1, three different subregions will be analyzed in detail, namely (i) the
 255 English Channel (6.5° W to 2° E - 48.5° N to 51° N), (ii) the Bay of Brest (6° W to 4° W -
 256 48° N to 48.5° N) and (iii) the Bay of Biscay (7° W to 0° W - 43° N to 48° N). This will allow
 257 us to explore these regions separately and highlight regional patterns. Those three subregions
 258 can be associated with three contrasted hydrodynamical regimes: macrotidal (English
 259 Channel), semi-enclosed bay (Bay of Brest), mesotidal (Bay of Biscay; Charria et al., 2013).

260

261 3. Results

262

263 3.1 Evolution of marine heatwave activity

264

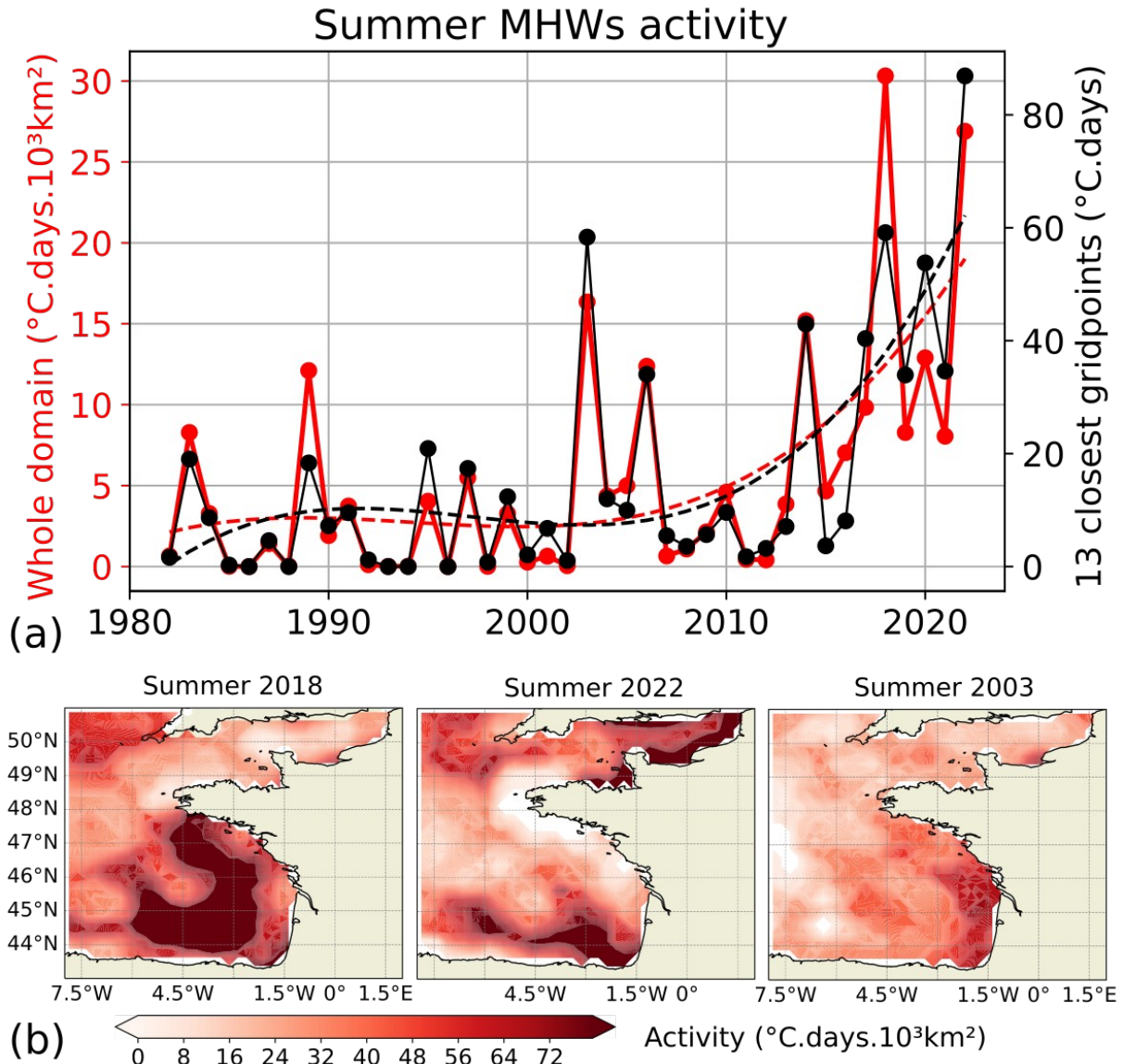
265 3.1.1. An integrated regional view

266

267 MHWs were detected over the Northeast Atlantic. The activity index (Figure 2a)
 268 highlights two main periods in the MHWs dynamics. Before 2003, MHWs activity remained
 269 moderate to weak with activity generally lower than 5 °C.days.10³ km² corresponding to 1.2
 270 mean occurrences per summer with a mean duration limited to 8 days (Figure 3). Only the
 271 summer of 1989 displayed strong MHWs activity (exceeding 10 °C.days.10³ km²) before
 272 2000. From 2003 onward, the activity increased over 30 °C.days.10³ km² for summers 2018
 273 and 2022 associated with more than 2.5 mean occurrences lasting around 20 days. The mean
 274 intensity remains quasi-steady during the whole period. The interannual variability and trend
 275 of the summer MHWs activity for the whole domain is similar to the one obtained for the
 276 average activity of the 13 grid cells closest to the buoy locations (black line of Figure 2),
 277 suggesting that at first order of magnitude, coastal and open ocean follow the same evolution.

278

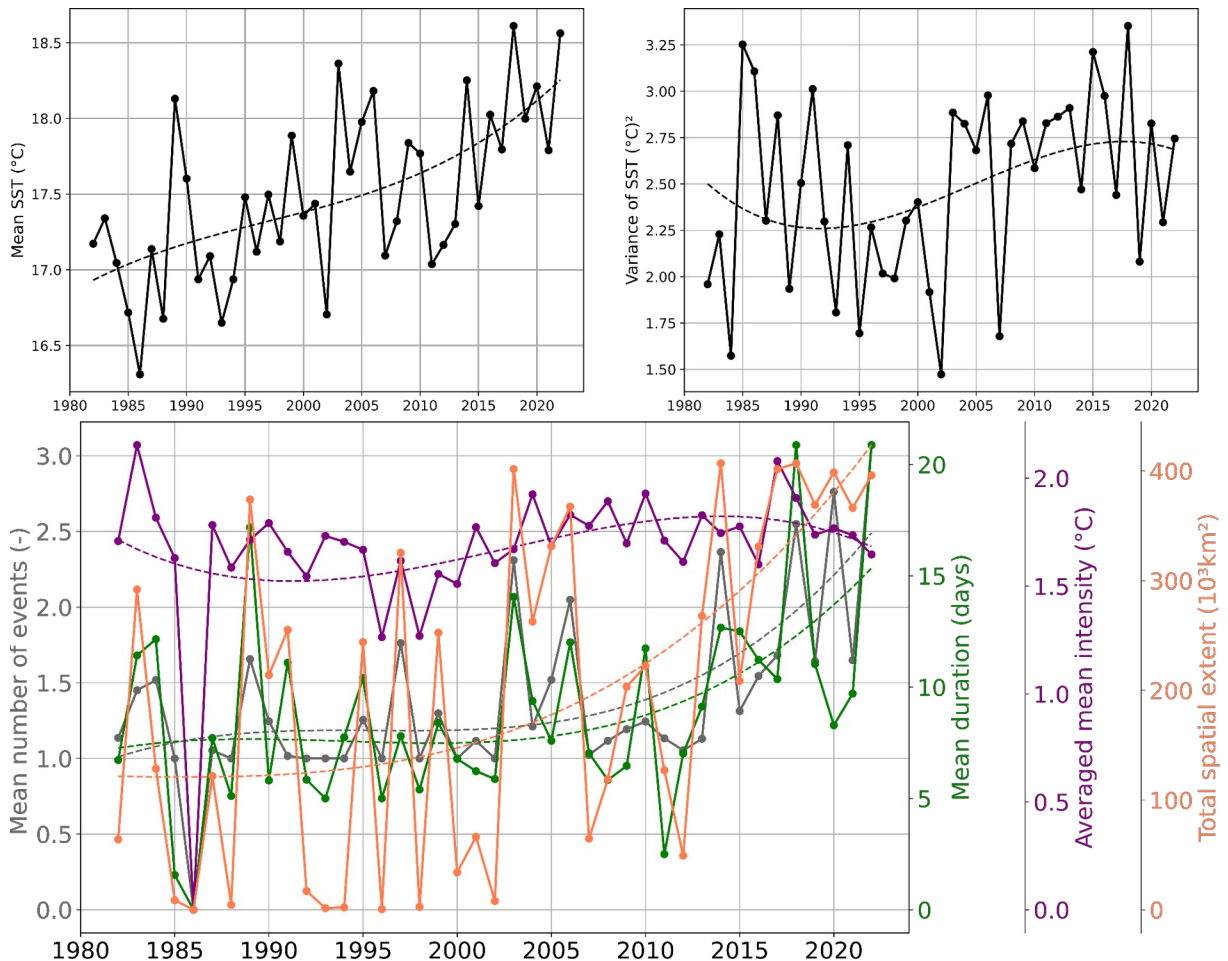
279



280
281 Figure 2: (a) Times series of summer (JJAS) MHWs mean activity in the Northeast Atlantic
282 from the satellite product (red curves) and for the average of the 13 grid cells closest to the
283 buoys from the satellite product (black curves). Dash lines represent the regression of a third-
284 order polynomial of the solid line with the same color. (b) Summer (JJAS) activity (first row;
285 in $^{\circ}\text{C.days}\cdot 10^3\text{ km}^2$) for the top 3 summers in terms of activity in the Northeast Atlantic (from
286 left to right).

287
288 The three most active summers are 2018, 2022 and 2003 (Figure 2a). During 2018
289 (Figure 2b), maximum activity is located in the Bay of Biscay over the outer continental shelf
290 and the continental slope from the southern part of the Biscay. These events are also
291 extending to the North until the South of Brittany and is limited by the Ushant tidal front (Le
292 Boyer et al., 2009; Müller et al., 2010) developed during summer. Regions of minimum
293 activity during 2018 are West of French Brittany in the Ushant front region where tides are
294 efficiently vertically mixing the water column. Similarly, the activity remains weak in the
295 English Channel, as it is a macrotidal region. In terms of duration, longer events are observed
296 in the Southern part of the Bay of Biscay exceeding 30 days (Figure S1). The 2022 summer is
297 the second most active year for the whole domain, with over $25\text{ }^{\circ}\text{C.days}\cdot 10^3\text{ km}^2$, and also the
298 strongest in terms of marine activity over coastal regions as shown by the maximum value of
299 the average activity near the 13 buoys considered (Figure 2a). Spatially, the English Channel

300 and the North of Spain record the strongest MHWs activity while the French Brittany coast
 301 has no occurrence over this year (Figure 2b). In the English Channel, the mean duration of the
 302 summer 2022 events was around 35 days (Figure S2) with localized events lasting more than
 303 50 days (Figure S1). In Northern Spain, the duration of the events was around 20 days,
 304 however, they occurred very frequently over the summer with strong mean MHWs intensities
 305 of around 2 °C (Figure S1). In 2003 (Figure 2c), the MHWs activity spatial distribution was
 306 different than in 2018 and 2022. The activity is larger over the inner continental shelf along
 307 Western French coasts in the Bay of Biscay. This region is under the influence of main river
 308 plumes along this coast (Adour, Gironde and Loire rivers). During this year, river discharge
 309 could have induced stratification (inducing faster warming of the surface mixed layer in
 310 regions of freshwater influence; Oh et al., 2023) and warmer waters from rivers suggest that
 311 observed MHWs were sustained by an atmospheric event more centered over lands. During
 312 this summer, the number of events is larger in the Western English Channel but shorter and
 313 less intense than in the Bay of Biscay. These top three active summers highlight the
 314 interannual spatial variability of MHWs activity. The detailed mean features (number of
 315 events, duration and mean intensity) of summer MHWs over the period 1982-2022 in the
 316 Northeast Atlantic, English Channel, Bay of Brest and Bay of Biscay are documented in
 317 Table S2.
 318



319 Figure 3: Time series of the mean (upper-left) and variance (upper-right) of SST (black curve)
 320 of summers (JJAS) over the Northeast Atlantic for the period 1982-2022. The SST variance is
 321 calculated for each year over the respective domain and measures the spread of the spatial
 322 distribution. (Bottom) Mean properties of summer (JJAS) MHWs in the Northeast Atlantic.
 323 The mean number of events (grey curve) is the number of events within the summer averaged
 324

325 over the domain (without considering cells with zero event). Mean duration (green curve) is
326 the average duration of every event within the summer and domain. Averaged mean intensity
327 (purple curve) is the average of the mean intensity of every event within the period and
328 domain. Total spatial extent (orange curve) is the sum of each grid cell area where one or
329 more events occur. If more than one MHWs occurs on the same cell, only one grid cell area is
330 taken into account. Dash lines represent the regression of a third-order polynomial of the solid
331 line with the same color.

332

333 The mean SST has been increasing over the 40 years with an approximately linear
334 trend, showing a mean warming of nearly 1.5 °C for the whole domain since 1982 (Figure 3).
335 Regionally, it is observed that the increase in the mean SST is almost yearly constant for the
336 Bay of Biscay region, and quadratic for the English Channel and Bay of Brest, where a
337 plateau is observed around 1995-2010 (Figure S2).

338

339 The SST variance is calculated for each year over the respective domain and measures
340 the spread of the spatial distribution. Over the Northeast Atlantic, during 1985-2002 and the 5
341 most recent years are characterized by a decline in the SST variance, while around 1992-2017
342 an increase in the SST variance is observed. This interannual trend is similar to the ones
343 observed for the events' intensity, with the exception of the English Channel, showing a direct
344 relationship between the SST variance and the mean intensity of the MHWs events. In the
345 English Channel, Bay of Brest and Bay of Biscay, the mean SST is warming and the variance
346 is increasing. This estimation points that they both contribute to the changes in the respective
347 MHWs activity (Figure S2).

348

349 Contributing to this recent increase in the Northeast Atlantic is primarily the sharp
350 trend of the events' spatial extent (~ 180 to 400 °C.days. 10^3 km²), followed by the rise of the
351 number of events (1.2 to 2.5) and also their duration (7 to 15 days; Figure 3). One should note
352 that, for the same number of events, the events' spatial extent can differ depending on their
353 spatial repartition, as in the events' spatial extent only one grid cell area is taken into account
354 when more than one event occurs on the same grid. Furthermore, over the most recent years
355 the mean number of events, their mean duration and total spatial extent reached the maximum
356 recorded values. Since 2017, the total spatial extent over the Northeast Atlantic has recorded
357 consecutive high values, exceeding 360.10^3 km². The summers of 2018, 2020 and 2022
358 recorded on average more than 2.5 events for almost all subregions, with events lasting on
359 average more than 20 days in 2018 (Bay of Biscay) and 2022 (English Channel; Figure S2).
360 Among the three studied subregions, the English Channel is the region experiencing the
361 strongest increase in summer MHWs activity over the last four decades (see trend in Figure
362 S3). The longest mean duration is seen in the English Channel (35 days in summer 2022), the
363 highest mean number of events occurred in the Bay of Brest (2.7 in summer 2020) and the
364 highest mean intensity is present in the Bay of Biscay (2.2 °C in 2017; Figure S2).

365

366 3.1.2. Coastal MHWs activity

367

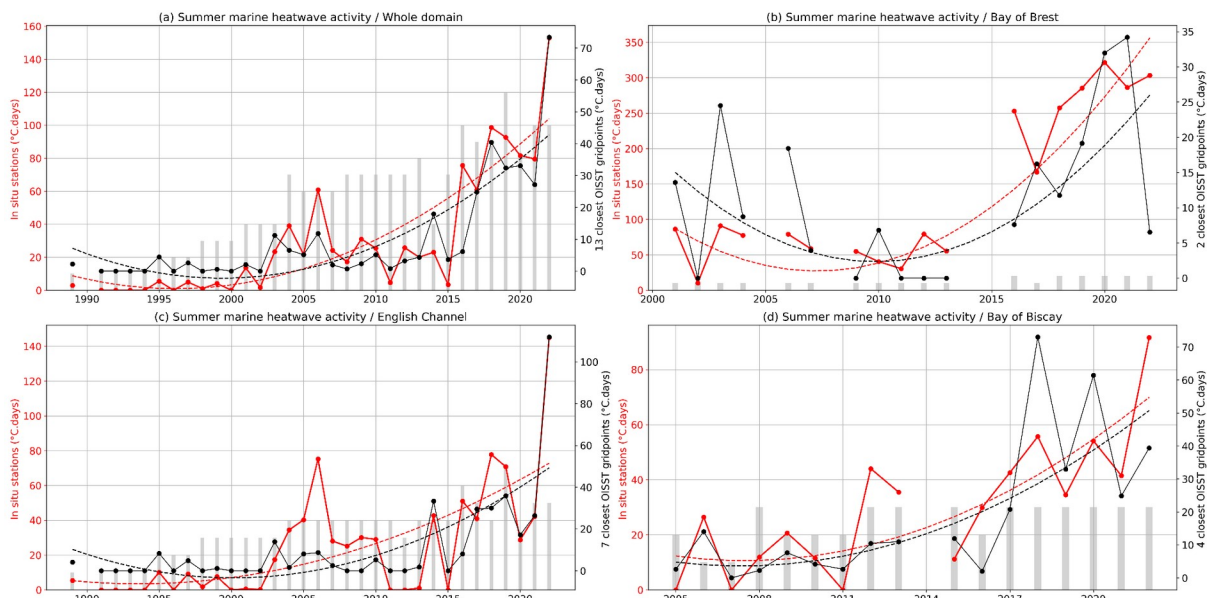
368 The spatial heterogeneity of the MHWs occurrence and activity can influence the
369 impact of MHWs along the coastline. We then explore MHWs activity detected along the
370 coast from *in situ* observations compared with remotely sensed observations. Figure 4 shows
371 the activity detected for the whole Northeast Atlantic domain and in the three subregions
372 where long-term *in situ* observations exist. To compare *in situ* and satellite data, for each
373 station, time series based on satellite data consider only years where *in situ* data exists (see
374 Table S1 for the starting date) and exceeds 80% of available data for the considered season.
Linked with the whole domain activity (Figure 4a), we observe an increase in the MHWs
activity in the three subregions (Figure 4b, c, d). Similar evolutions are observed when the

375 satellite product or coastal buoys are considered. In the Bay of Brest, we also observe a
 376 similar increase but with larger activity in *in situ* observation as the intensity of extreme is
 377 underestimated by the satellite in this semi-enclosed bay. The use of *in situ* observation is
 378 limiting the length of the analyzed time series. However, we can observe larger activity in
 379 recent years from both datasets. For most cases, similar most active years are detected with *in*
 380 *situ* observations and satellite data.

381 Considering coastal stations over the observed periods, we see a more pronounced
 382 increase in MHWs activity from 2010. The English Channel and the Bay of Biscay *in situ*
 383 stations highlight the year 2022 as the most active year exceeding 140 °C.days. In the Bay of
 384 Brest, the impact of the 2022 MHWs is less pronounced, in agreement with satellite
 385 observation (Figure 2b) due to tidally driven vertical mixing.

386 When we compare MHWs activity estimated from *in situ* stations and satellite product, values
 387 are generally larger from *in situ* stations. Those differences are explained by the
 388 underestimation of extreme temperatures in coastal regions in remotely sensed products.
 389

390



391

392 Figure 4: Time series of summer (JJAS) MHWs mean activity (a) in the whole domain
 393 (Northeast Atlantic) and in three subregions: (b) Bay of Brest, (c) the English Channel, and
 394 (d) Bay of Biscay. The red curve represents the activity based on *in situ* observations. The
 395 black curve represents the activity based on satellite dataset for the closest non-masked points
 396 with *in situ* stations when *in situ* data exists. Dash lines represent the regression of a third-
 397 order polynomial of the solid line with the same color. Grey bars are proportional to the
 398 number of considered *in situ* time series. MHWs activity from *in situ* time series with less
 399 than 80% of observation during the analyzed season is not computed.

400

401 3.2 Evolution of marine cold-spell activity

402

403 3.2.1 An integrated regional view

404

405

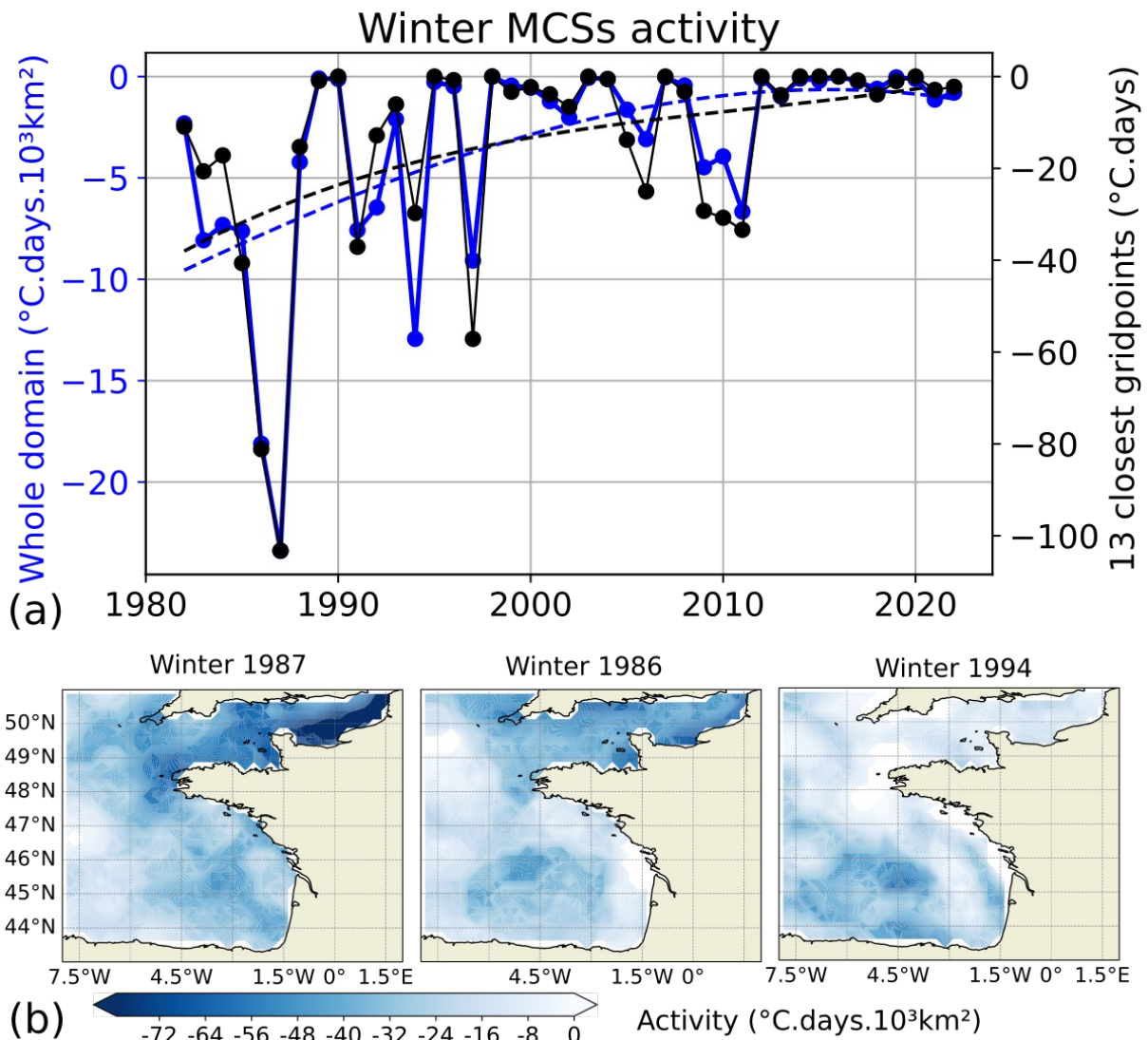


Figure 5: Same as Figure 2 but for MCSs in winter (DJFM).

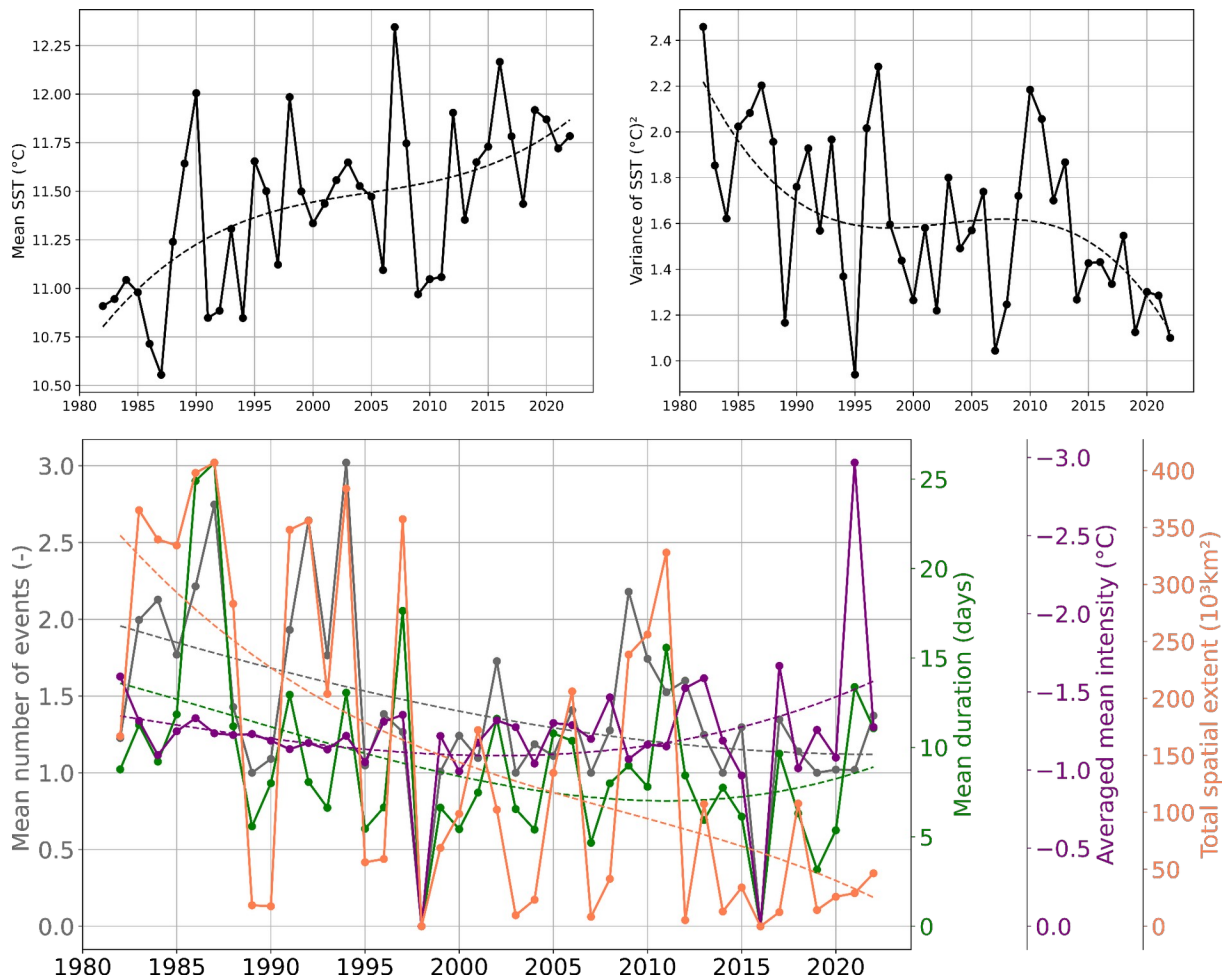
Figure 5 depicts winter MCSs evolution for the whole domain over the last four decades (1982-2022). MCSs activities decrease linearly during the first half of the period, showing almost no occurrence after 2000 with the exception of 2006 and 2009 to 2011. A similar evolution is seen by considering the average of the 13 grid points closest to each *in situ* station.

The three most active MCSs occur in winter 1987 ($-24\text{ }^{\circ}\text{C.days.}10^3\text{km}^2$), 1986 ($-18\text{ }^{\circ}\text{C.days.}10^3\text{km}^2$) and 1994 ($-13\text{ }^{\circ}\text{C.days.}10^3\text{km}^2$). In the two coldest winters, MCSs were dominant in the English Channel, especially off the Northern French Coast in winter 1987. These two winters are characterized by long (~ 50 days) and intense ($\sim -2.5\text{ }^{\circ}\text{C}$ anomalous SST) and few events (~ 1 event; Figure S4). This region is subject to high turbulent mixing generated by the tidal current, which could favor cold conditions. By contrast to these two winters (1987 and 1986), winter 1994 featured strong MCSs activity in the center of the Bay of Biscay, due to numerous (~ 5 events) but moderate intensity ($\sim -1.3\text{ }^{\circ}\text{C}$) and relatively short (20 days) events. The three winters 2009-2011 present very localized extreme cold conditions along the coastal Armorican Shelf, and additionally in the English Channel for 2011 (not shown). The detailed mean features (number of events, duration and mean intensity) of winter

426 MCSs over the period 1982-2022 in the Northeast Atlantic, English Channel, Bay of Brest
 427 and Bay of Biscay are documented in Table S3.

428

429



430

431

432 Figure 6: Same as Figure 3 but in winter (DJFM) and MCSs (blue curve)

433

434

435

436

437

438

439

440

441

442

443

444

445

446

447

448

449

The mean and variance evolution of SST, as well as the mean evolution of MCSs properties (occurrence, duration, mean intensity and spatial extent) are presented over the whole domain (Figure 6) and separately for the English Channel, the Bay of Brest and the Bay of Biscay (Figure S5). Over the whole Northeast Atlantic domain, the SST mean increases and spatial dispersion (variance) decreases with both a plateau around 1995-2010, following the English Channel and the Bay of Biscay evolution. On the contrary, a steady increase in the mean SST and a nearly constant variance of SST is seen in the Bay of Brest.

The warmer winter seen over the whole domain and for the three subregions is consistent with the decrease of the extremely cold conditions, depicted by the mean MCSs activity. The decrease in the mean MCSs activity is controlled by the strong decrease in spatial extent (350 to 50 10^3 km^2), the moderate decrease in the number of events (2 to 1.2 events), and the small decrease in duration (13 to 9 days). The mean intensity does not show any trend ($\sim -1.5 \text{ }^\circ\text{C}$).

The decrease of spatial dispersion (variance) of SST over the whole domain indicates a more uniform evolution which is explained by a dominant warming trend stronger for colder areas. Indeed, the relatively cold English Channel's temperature increased by $1.5 \text{ }^\circ\text{C}$ (from 9

450 °C to 10.5 °C) and the relatively warmer Bay of Biscay increased by 0.8 °C (from 11.8 °C to
451 12.6 °C) over the 1982-2022 period. When considering individually the three subregions,
452 localized enough to be under a similar trend, the variance also decreases (Figure S5). The
453 decrease of variance is more pronounced for the English Channel than for the Bay of Brest
454 and Bay of Biscay. Therefore, a first estimate shows that mean SST warming and the variance
455 changes both contribute to the changes in MCSs activity in the English Channel, Bay of Brest
456 and Bay of Biscay.

457 MCSs activity generally follows the SST evolution, albeit with small differences.
458 Indeed, winter 1991 and 1994 have a similar mean SST (10.8 °C) but the MCSs activity is
459 three times higher in 1994 than in 1991, driven by a higher number of events (3 instead of 2
460 events with similar duration, mean intensity and spatial extent).

461 Even if changes in winter occur in the Bay of Brest and Bay of Biscay, more drastic
462 changes are seen in the English Channel over the period 1982-2022 (see trend in Figure S6).
463 In the English Channel, the trend of MCSs shows at the beginning of the period, a mean
464 occurrence of 2 events/winter, lasting 15 days with a mean intensity of -1.5 °C over an area of
465 $100 \cdot 10^3 \text{ km}^2$, followed by a sharp decline ending to no detected MCSs in the last four years
466 (2019-2022). In the Bay of Brest over the same period, MCSs properties decrease from 1.5
467 events during 15 days at a mean intensity of -1.4 °C over $11 \cdot 10^3 \text{ km}^2$ to 0.5 events during 8
468 days at a mean intensity of -0.8 °C over $0.5 \cdot 10^3 \text{ km}^2$. Exceptional long events occurred in the
469 winter of 1987 with a mean duration of 55 days. In the Bay of Biscay, the MCSs decline in
470 occurrence (from 2 to 1 event), duration (from 11 to 9 days) and spatial extent (170 to $40 \cdot 10^3$
471 km^2) while the mean intensity rises from -1.3 °C to -1.5 °C. The increase is explained by
472 winter 2021; without these events, the mean intensity would have been nearly constant around
473 -1.3 °C. Indeed, winter 2021 shows a small activity but the highest mean intensity (-3 °C over
474 the whole domain) which is explained by a localized event in the coastal area off South-West
475 of France with a maximum intensity of (-5.6 °C). Apart from a very intense and localized
476 event in the coastal area off South-West of France in winter 2021 and a very long event in the
477 Bay of Brest in winter 1987, severe MCSs occurred predominantly in the English Channel
478 (winter 1987 and 1986).

479

480

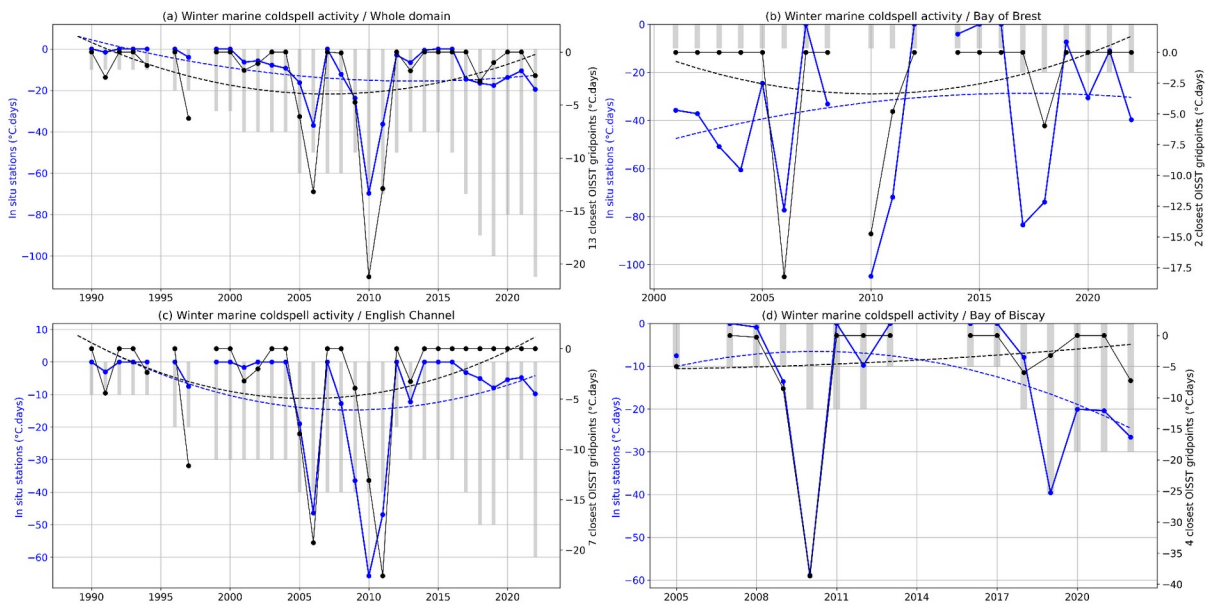
481 3.2.2. Coastal MCSs activity

482

483 Figure 7 shows the time series of MCSs activity for *in situ* data and satellite data
484 considering the same missing data as each *in situ* station data. Along the coasts, MCSs
485 activity as determined by local buoys remains weaker than MHWs activity as defined using
486 satellite data. As for the MHWs, MCSs intensity is underestimated in satellite observations
487 but evolutions are similar. From *in situ* observations from coastal stations, two years can be
488 highlighted due to their intense MCSs: 2006 and 2010 (Figure 7). The year 2010 is the most
489 intense, in terms of MCSs. The mean activity is reaching -100 °C.day in the Bay of Brest and
490 around -60 °C.day in the Bay of Biscay and the English Channel. In 2006, the activity was
491 also important compared with other years: around -80 °C.day in the Bay of Brest and around -
492 50 °C.day in the English Channel. This extreme year 2006 was also unique with a peak in
493 MHWs activity during the summer (Figure 4). Before the year 2000, only observed in the
494 English Channel from coastal stations, three other years reveal intense MCSs activity: 1997,
495 1991, 1994 (from the most intense to the less active winter) from satellite data at the closest
496 point of *in-situ* data.

497 We do not detect a significant trend in the interannual evolution of MCSs activity
 498 along the coasts. For the Bay of Biscay and the Bay of Brest, it can be directly connected to
 499 the lack of observation before 2000 when the largest MCS occurs. In the English Channel, the
 500 lack of observation also explains the observed lack of trend. Indeed, only one time series was
 501 available before 1995 and this station (GREENwich) is not detecting an important MCSs
 502 activity before 2000.

503
 504
 505



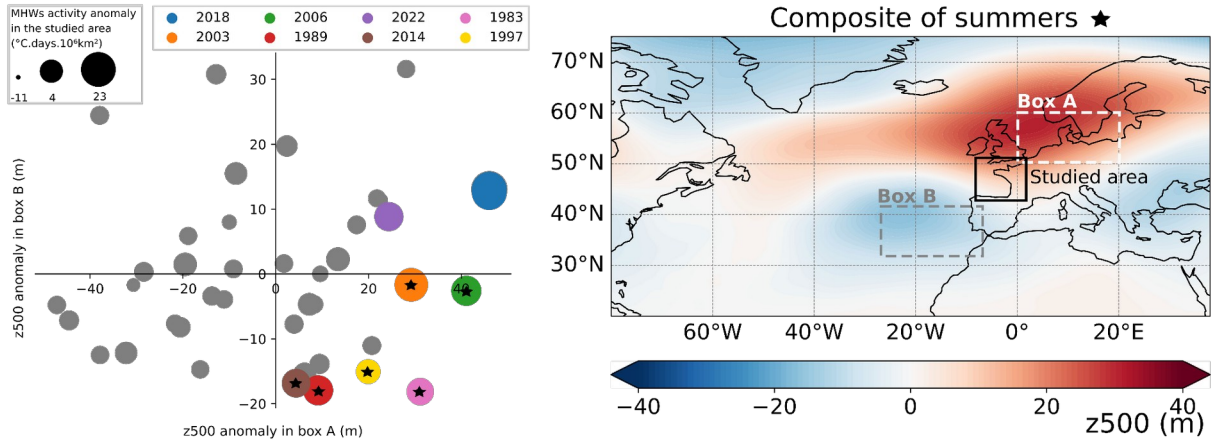
506
 507 Figure 7: Same as Figure 4 but for MCSs in winter (DJFM).
 508

509 3.3 Associated atmospheric patterns 510

511 Apart from the long-term trend of increasing SST, we also see high interannual
 512 variability which is potentially connected with atmospheric forcing modes (Holbrook et al.
 513 2019; Izquierdo et al., 2022a). Figure 8 presents the atmospheric circulation in the North
 514 Atlantic associated with strong interannual MHWs in the Bay of Biscay and the English
 515 Channel. For each summer of the 1982-2022 period, MHWs total activity anomaly in the
 516 studied area box (Northeast Atlantic) with respect to the third-order long-term trend (red
 517 dotted curved in Figure 2a) was computed. This anomaly represents the detrended or
 518 interannual MHWs activity. Eight summers were identified as having high interannual
 519 activities (anomalous total activity exceeding a threshold of $4 \text{ } ^\circ\text{C}\cdot\text{days}\cdot 10^6\cdot\text{km}^2$, coloured
 520 marker in Figure 8 left panel). The year 2018 ($23 \text{ } ^\circ\text{C}\cdot\text{days}\cdot 10^6\cdot\text{km}^2$), 2003 (17
 521 $^\circ\text{C}\cdot\text{days}\cdot 10^6\cdot\text{km}^2$) and 2006 ($12 \text{ } ^\circ\text{C}\cdot\text{days}\cdot 10^6\cdot\text{km}^2$) are the three strongest summers. Six out of
 522 these eight summers (all except 2018 and 2022) have an anomalous geopotential height at 500
 523 hPa which is positive over Northern Europe (box A in Figure 8) and negative in the West of
 524 the Iberian Peninsula (box B in Figure 8). The composite of the anomalous geopotential
 525 height at 500 hPa for these six summers shows in the North Atlantic-Europe sector a positive
 526 summer NAO-like pattern, with a high over the Nordic sea and two lows over the Iberian
 527 Peninsula and Greenland. This overall result is not sensitive to small displacements of boxes
 528 (a few latitude and longitude degrees; not shown).

529
 530
 531

532



533

534

535

536

537

538

539

540

541

542

543

544

545

546

547

548

549

550

551

552

553

554

555

556

557

558

559

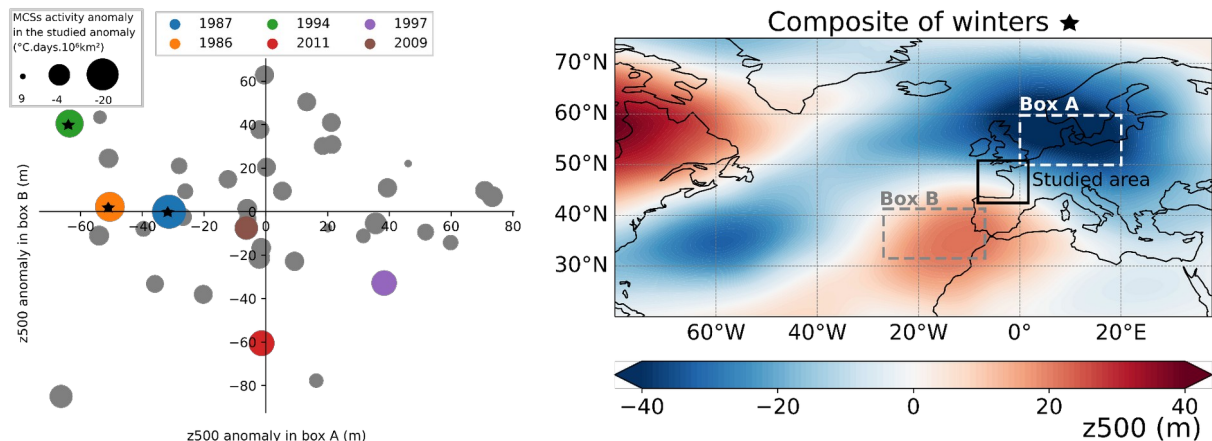
560

561

562

Figure 8: (Left panel) Scatter plot of anomalous summer (JJAS) geopotential height at 500 hPa (z500; in m) in box A versus the anomalous geopotential height at 500 hPa in box B with respect to the summer period 1982-2022. The size of the marker is proportional to the anomalous summer (JJAS) MHWs total activity, calculated as the sum of all grid point activity in the studied area (in $^{\circ}\text{C}\cdot\text{days}\cdot 10^6\cdot\text{km}^2$) with respect to the trend (red dotted curved in Figure 2a). Markers are in color when this value exceeds $4\text{ }^{\circ}\text{C}\cdot\text{days}\cdot 10^6\cdot\text{km}^2$ and the stars are indicated when markers in color are in the lower-right “cluster” of the graph. (Right panel) Composites of summers (JJAS) marked with stars in the left panel of the anomalous geopotential height at 500 hPa (m) with respect to the summer period 1982-2022. Box A is the domain 0°E to 20°E - 50°N to 60°N and box B is the domain 33°W to 13°W - 31°N to 41°N .

Summer (JJAS) 2018 has the strongest anomalous MHWs activity in the Northeast Atlantic but, at the difference to the six next summers in the ranking of detrended MHWs activity, does not present a decrease in the geopotential height at 500 hPa in the West of Iberian Peninsula (box B). A broad high-pressure system in the North Atlantic-European sector is seen (including box A), except in the Eastern Mediterranean and up to 60°N where a low occurs (Figure S7). This response in box B for summer 2018 is primarily due to late summer (August and September) atmospheric circulation (Figure S7). These months have a minor contribution to MHWs total activity for the whole summer (JJAS; Figure S8). When considering the month of June, with 2018 MHWs peaks (Figure S8), the North Atlantic shows a positive summer NAO regime, similar to the next six summers' highest MHWs activity. This analysis demonstrates that MHWs in the Northeast Atlantic is closely associated with a high-pressure system over Northern Europe, and a low off the Iberian Peninsula, resembling the positive phase of the summer NAO. By performing this analysis with SST instead of MHWs activity, we obtain similar results, albeit with a less extended high over Northern Europe (Figure S9).



563
 564 Figure 9: Same as Figure 8 but for MCSs in winter (DJFM). MCSs anomalies are calculated
 565 with respect to the third-order trend (blue dotted curved in Figure 5). Markers are in color
 566 when this value is below $-4 \text{ } ^\circ\text{C.days.10}^6.\text{km}^2$ and stars are indicated when markers in color
 567 are in the upper-left section of the graph.

568 Regarding MCS, the three highest detrended MCSs activities are winter 1987 (-20
 569 $^\circ\text{C.days.10}^6.\text{km}^2$), 1986 ($-13 \text{ } ^\circ\text{C.days.10}^6.\text{km}^2$) and 1994 ($-10 \text{ } ^\circ\text{C.days.10}^6.\text{km}^2$; Figure 9).
 570 These three most active winters are in the same “cluster”, with an anomalous geopotential
 571 height at 500 hPa negative over Northern Europe and positive in the West of the Iberian
 572 Peninsula. Composite of the anomalous geopotential height at 500 hPa for these three winters
 573 shows in the North Atlantic-Europe sector a broad and strong low in Northern Europe, a
 574 weaker low-pressure system sitting in the Northwest Atlantic, and two highs off the Iberian
 575 Peninsula and over the Hudson Bay. This analysis suggests that extreme MCSs in the
 576 Northeast Atlantic might be closely associated with a low over Northern Europe and a high
 577 off the Iberian Peninsula. By performing this analysis with SST instead of the MCSs activity
 578 (Figure S10), the result are sparse, showing only winter 1986 as strong anomalous cold SST
 579 linked to an anomalous geopotential height at 500 hPa over Northern Europe and positive in
 580 the West of the Iberian Peninsula.

581 When comparing the anomalous geopotential height conditions for the most intense
 582 summer MHWs and winter MCS, we see that the geopotential height conditions are somehow
 583 opposite, although the amplitude is stronger for winter, consistent with stronger climatology
 584 (Folland et al., 2009). However, while summer MHWs are associated with a positive summer
 585 NAO, winter MCSs do not present a negative winter NAO general pattern.

586 To provide indications on the drivers of these events, we have considered the different
 587 components of air-sea heat flux anomalies concomitant with MHWs and MCSs. For the eight
 588 most severe interannual summer MHWs (see marker in color Figure 8) and the six most
 589 severe interannual winter MCSs (see marker in color Figure 9), the anomalous (i) short-wave
 590 radiation flux, (ii) surface net long-wave radiation flux, (iii) surface sensible heat flux and (iv)
 591 latent heat flux are depicted, respectively Figure S11 and Figure S12. The interannual (or
 592 detrended) summer MHWs are predominantly driven by high short-wave radiation flux,
 593 except for years 1983 and 1997 that only shows important positive downward latent heat flux.
 594 The other air-sea flux have a smaller contribution. The interannual winter MCSs seem to be
 595 mostly driven by high sensible heat flux and low short-wave radiation flux. This suggests that,
 596 in this region, low cloud cover is a key parameter for the generation of summer MHWs while
 597 strong winds and high cloud cover are important for the apparition of winter MCSs. Further

598 analysis needs to be done to attribute quantitatively the contribution of each air-sea heat flux
599 component.

600 **4. Discussion**

601

602 In the Northeast Atlantic, an increase in the MHWs activity and a decrease in MCSs
603 activity were observed. Interannual changes confirm that general large scale trends (Oliver et
604 al., 2018; Schlegel et al., 2021) are also observed in regions where the coastal hydrodynamics
605 could limit the impact due to active vertical mixing processes (*e.g.* barotropic and internal
606 tides, wind-driven mixing in shallow waters).

607 The most active summer MHWs analyzed over the Northeast Atlantic and in the
608 period 1982-2022 occurred in the Bay of Biscay (2018) and the most active winter MCSs
609 occurred in the English Channel (1987). This is consistent with Schlegel et al. (2021) who
610 found that the maximum intensity of MHWs dominates MCSs in the Bay of Biscay, and vice
611 versa in the English Channel. Along the coasts, the maximum of MHWs activity is detected in
612 2022 in the English Channel which might be related to the summer European heatwaves
613 recorded (ECMWF, 2022; Savu, 2022; Guinaldo et al., 2023).

614 In the Bay of Biscay, we see a linear warming rate in summer since the beginning of
615 the studied period. This is in accordance with DeCastro et al. (2009) which shows a steady
616 linear warming rate since the 1970s, based on data from 1854-2006. Mean SST together with
617 SST variance increase justify the rise of MHW. This increase of MHWs is consistent with
618 Izquierdo et al. (2022a) who determined more precisely an equal contribution of each of these
619 two factors for the South coast of the Bay of Biscay. This is specific to this region (as well as
620 for the Bay of Brest and the English Channel), as for most of the other regions of the world,
621 the mean warming and not the SST variability changes contribute to the increase in MHWs
622 features (Alexander et al., 2018; Oliver et al., 2020). Besides, we found a positive trend for
623 the MHWs activity parameter using both satellite data and the 4 buoys in the Bay of Biscay,
624 and for the duration and occurrence using satellite data. The trends are quasi-similar
625 considering only the two buoys on the South coast of the Bay of Biscay (GIJO and BILB) and
626 the two on the West coast of the Bay of Biscay (ARCA and MOLI; not shown) and are
627 marked by the high activity present in the more recent summers. This evolution in the
628 occurrence and duration of MHWs were not seen in Izquierdo et al. (2022b) using two buoys
629 in the South coastal Bay of Biscay over the period 1998-2018, which could be explained by
630 local process or studied season (March to August).

631

632 The results from *in situ* and satellite datasets for each of the studied regions are quite
633 in agreement, albeit the satellite underestimates the amplitude of activity for both MHWs and
634 MCS. Conversely, Izquierdo et al. (2022a) found an overestimation of the MHWs using
635 satellites compared to *in situ* in the coastal upwelling region South of the Bay of Biscay,
636 which might be related to local processes. The satellite's coarse resolution mostly (i) smoothes
637 small-scale and short events and (ii) interpolates with offshore regions, having greater thermal
638 inertia (Marin et al., 2021) which can lead to the overestimation of the duration of events and
639 the underestimation of the intensity. However, we show that coastal *in situ* stations distributed
640 along the Northeast Atlantic coasts allow the detection of large-scale evolutions of MHWs
641 and MCSs activity. Analyzed locally, they can also inform on evolutions related to local
642 hydrodynamics.

643

644 Internal variability of winter MCSs is related to low pressure over Northern Europe
645 and a high-pressure West of the Iberian Peninsula for three (1987, 1986 and 1994) out of the
646 six most intense events. Among other strong interannual MCSs, winter 2011 does not present

647 this pattern but could have been generated by a cold air outbreak brought by a ridge over
648 Greenland (Norris et al., 2013). A relation at an interannual timescale could exist between
649 MCSs (Figure 7, middle panel) and extreme low-salinity events (Poppeschi et al., 2021) in
650 winter in the Bay of Brest, as, using the same *in situ* buoys (COAST-HF-Iroise from 2000-
651 2018), two out of the four most severe low-salinity events are concomitant with MCSs (winter
652 2001 and 2007). These extreme events could be both influenced by intense mid-latitude
653 depressions, but river discharges are also an important driver in this region. Unlike MHWs
654 (Figure 2), extreme cold conditions occurred several winters in a row: three in 2009-2011 and
655 two in 1986-1987. This might be explained by the re-emergence of cold water originating
656 from the previous winter, as for the 2013-2016 north Atlantic cold Blob (Duchez et al., 2016a;
657 Josey et al., 2018; Schlegel et al., 2021).

658

659 Summer 2018 presents the most active MHWs in the Northeast Atlantic for the period
660 1982-2022, consistent with the reported warmer SST (+1 to +3 °C above the long-term
661 climatology) the same summer in the proximity of the United Kingdom (McCarty et al.,
662 2019). On the continental side, this summer was also recorded as the hottest in the United
663 Kingdom since 1884 (McCarty et al., 2019) and one of the hottest over northwestern Europe
664 (Met Office, 2018; Météo-France, 2018). On top of the underlying warming climate forcing
665 (Vogel et al., 2019; Yiou et al., 2020), this extreme continental warm conditions in 2018 have
666 been previously reported as a consequence of the positive summer NAO anomalies combined
667 with elevated SST (McCarty et al., 2019) or combined with stationary Rossby waves in
668 synoptic anomalies (Drouard et al., 2019; Kornhuber et al., 2019). More generally, the
669 positive phase of the summer NAO is associated with warm anomalies from the West of the
670 United Kingdom to the Baltic (Folland et al., 2009). Our findings on the ocean side
671 corroborate the continental counterpart as extremely warm conditions in the Bay of Biscay
672 and the English Channel are likely associated with positive summer NAO, consistent with the
673 result of Holbrook et al. (2019).

674

675 Depending on the region and the event, MHWs can be associated with anomalous air–
676 sea heat fluxes which can include high short-wave, due to less cloud cover and greater
677 insolation, high sensible heat fluxes when the surface air is warm and/or low latent heat loss
678 from the ocean, due to weak winds (Oliver et al., 2021). In the English Channel and the Bay
679 of Biscay, Guinaldo et al. (2023) linked the summer of 2022 sea-surface temperature to
680 abnormally high short-wave radiation in the Bay of Biscay and English Channel. In this study,
681 a similar conclusion is found by considering the eight most severe interannual MHWs in the
682 Northeast Atlantic (which includes the English Channel and the Bay of Biscay, and summer
683 of 2022). Abnormally high short-wave radiation is likely associated with reduced cloudiness
684 and Folland et al. (2009) have found that during the positive index phase of the summer NAO,
685 northwest Europe experiences significantly reduced cloudiness. This is consistent with our
686 suggestion that the positive phase of the summer NAO favours the generations of summer
687 MHWs in the Northeast Atlantic through reduced cloudiness. MCSs in the English Channel
688 are associated with high sensible heat flux, consistent with reported MCSs often driven by
689 strong winds in shallow waters, enabling a rapid chilling of the surface water (Crisp, 1964;
690 Schlegel et al., 2021). We also found a possible role of weaker short-wave radiation, which
691 might be related to increased cloud coverage.

692

693 In the future and under increasing greenhouse gas concentrations, climate models
694 predict that the ocean surface in the Bay of Biscay and the English Channel will continue to
695 warm (Fox-Kemper et al., 2021) and a trend toward a positive summer NAO pattern (Faranda
696 et al., 2019). Both these effects imply the long-term likelihood of increased MHWs in the

697 Northeast Atlantic, but to what extent are the long-term and the interannual variability
698 contributions remain to be shown. Also, the role of large-scale ocean circulation features,
699 such as the Shelf Edge Current (Alheit et al., 2019) or Iberian Poleward Current (Charria et
700 al., 2013), upper ocean preconditioning (Josey et al., 2018), and the importance of remote
701 large-scale climate modes of variability, such as the Indian Ocean Dipole (Holbrook et al.,
702 2019) in amplifying or suppressing MHWs occurrences in the Bay of Biscay and English
703 Channel would need specific investigation. Along the coasts, the role of main river inflow at
704 the land-sea continuum can also lead to specific answers on the coastal ocean to future climate
705 evolutions.

706
707

708 5. Conclusions

709

710 The activity index, a combination of the properties of marine extreme events, shows a
711 positive trend for summer MHWs in the Northeast Atlantic (since 2000 and more pronounced
712 since 2010) and in the three subregions, the English Channel, the Bay of Brest and the Bay of
713 Biscay for both *in situ* and satellite data. This is explained by both a mean and variance SST
714 increase. Conversely, a decrease in MCSs activity was detected, with almost no events after
715 2000, more clearly with the satellite data due to the longest time series (40 years) compared
716 with the *in situ* (20 to 30 years). These changes are fast for the three subregions, with the
717 English Channel being the subregion with the more drastic growth.

718 In the Northeast Atlantic, MHWs are more frequent, longer, and extend over larger areas,
719 while the opposite is seen for MCSs. For both MHWs and MCSs, the mean intensity shows
720 only weak changes over the last four decades.

721 Moreover, we found that the satellite dataset used is in good accordance with *in situ* data in
722 the Northeast Atlantic, except for the fact that satellites underestimate the amplitude of both
723 hot summer and cold winter marine extreme events in the coastal areas. The implemented *in*
724 *situ* stations appear as a well-designed observing system to detect the long-term evolution of
725 MHWs and MCSs activity and to document local features related to coastal hydrodynamics.

726

727 MHWs activity is particularly high in 2018 and 2022 through two different situations.
728 The year 2018 is characterized by a large extent of MHWs in the Bay of Biscay with long
729 events in the South of the Bay and intense events in the Armorican Shelf. The summer of
730 2022 features long MHWs mainly in the English Channel. MCSs activity is the highest in
731 1986 and 1987 due to long and intense events in the English Channel.

732 Our findings show that summers with strong MHWs activity due to internal variability
733 (after removing the trend) in Northeast Atlantic have often been associated with a ridge over
734 the northern Europe sea and a trough West of the Iberian Peninsula; the opposite situation is
735 seen for MCSs. In the case of MHW, the wide atmospheric pattern resembles the positive
736 phase of the summer NAO. This preliminary analysis of air-sea heat flux suggests that in the
737 Northeast Atlantic interannual (or detrended) summer MHWs are predominantly driven by
738 high short-wave radiation flux and interannual winter MCSs by high sensible heat flux and
739 low short-wave radiation. This suggests that, in this region, low cloud cover is a key
740 parameter for the generation of summer MHWs while strong winds and high cloud cover is
741 important for the apparition of winter MCSs. We caution that the proposed connection does
742 not necessarily indicate causal links but these relations can provide indications of drivers.

743

744 Despite contrasted hydrodynamical regimes (meso- and macro-tidal) and circulation
745 (shallow water under freshwater influence, shelf circulation, active sub-mesoscale), the
746 Northeast Atlantic region displays similar changes in MHWs and MCSs activity between

747 coastal and open ocean regions. Those changes need to be anticipated to mitigate the impacts
748 on coastal ecosystems.
749

750 **Acknowledgements**

751 This work was partially supported by national funds through FCT (Fundação para a
752 Ciência e a Tecnologia, Portugal) through project ROADMAP (JPIOCEANS/0001/2019). It
753 is also funded by the regional project (Contrat Plan Etat-Region) ObsOcean/ROEC-ILICO
754 and the regional COXTCLIM project funded by the Loire-Brittany Water Agency, the
755 Brittany region, and Ifremer. We thank Oregon Segalen for fruitful discussions. We thank
756 Tim Smyth for providing data from Western Channel Observatory. We acknowledge the
757 COAST-HF (<http://www.coast-hf.fr>) national observing network component of the National
758 Research Infrastructure ILICO.
759

760 **Declaration of competing interest**

761 The authors declare that they have no known competing financial interests or personal
762 relationships that could have appeared to influence the work reported in this paper.

763 **Authors contributions**

764 All authors contributed to the conception and design of the study. AS performed the
765 calculation and designed the figures involving the satellite dataset, GC and CP did so for the
766 *in situ* dataset. All authors contributed to the discussion, writing and review of the manuscript.
767

768 **References**

- 769
770
771 Alexander, M. A., Scott, J. D., Friedland, K. D., Mills, K. E., Nye, J. A., Pershing, A. J., &
772 Thomas, A. C. (2018). Projected sea surface temperatures over the 21st century: Changes in
773 the mean, variability and extremes for large marine ecosystem regions of Northern Oceans.
774 *Elementa: Science of the Anthropocene*, 6.
775
776 Alheit, J., Gröger, J., Licandro, P., McQuinn, I. H., Pohlmann, T., & Tsikliras, A. C. (2019).
777 What happened in the mid-1990s? The coupled ocean-atmosphere processes behind climate-
778 induced ecosystem changes in the Northeast Atlantic and the Mediterranean. *Deep Sea*
779 *Research Part II: Topical Studies in Oceanography*, 159, 130-142.
780 <https://doi.org/10.1016/j.dsr2.2018.11.011>
781
782 Barnston, A. G., & Livezey, R. E. (1987). Classification, seasonality and persistence of low-
783 frequency atmospheric circulation patterns. *Monthly weather review*, 115(6), 1083-1126.
784 <https://doi.org/10.1175/1520-0493>

- 785 Brown Ross, A., Lilley, M. K. S., Shutler, J., Widdicombe, C., Rooks, P., McEvoy, A.,
786 Torres, R., Artioli, Y., Rawle, G., Homyard, J., Tyler, C. R., & Lowe, C. (2022). Harmful
787 Algal Blooms and their impacts on shellfish mariculture follow regionally distinct patterns of
788 water circulation in the western English Channel during the 2018 heatwave. *Harmful Algae*,
789 *111*(December 2021), 102166. <https://doi.org/10.1016/j.hal.2021.102166>
- 790 Charria, G., Lazure, P., Le Cann, B., Serpette, A., Reverdin, G., Louazel, S., Batifoulier, F.,
791 Dumas, F., Pichon, A., & Morel, Y. (2013). Surface layer circulation derived from
792 Lagrangian drifters in the Bay of Biscay, *Journal of Marine Systems*, *109*, 60–76.
793 <https://doi.org/10.1016/j.jmarsys.2011.09.015>
- 794 Chust, G., Borja, Á., Caballero, A., Irigoien, X., Sáenz, J., Moncho, R., Marcos, M., Liria, P.,
795 Hidalgo, J., Valle, M., & Valencia, V. (2011). Climate change impacts on coastal and pelagic
796 environments in the southeastern Bay of Biscay. *Climate Research*, *48*(2–3), 307–332.
797 <https://doi.org/10.3354/cr00914>
- 798 Crisp, D. J. (1964). The Effects of the Severe Winter of 1962-63 on Marine Life in Britain.
799 *Journal of Animal Ecology*, *33*(1), 165-210, <https://www.jstor.org/stable/2355>
- 800 Darmaraki, S., Somot, S., Sevault, F., & Nabat, P. (2019). Past Variability of Mediterranean
801 Sea Marine Heatwaves. *Geophysical Research Letters*, *46*(16), 9813–9823.
802 <https://doi.org/10.1029/2019GL082933>
- 803 DeCastro, M., Gómez-Gesteira, M., Alvarez, I., & Gesteira, J. L. G. (2009). Present warming
804 within the context of cooling–warming cycles observed since 1854 in the Bay of Biscay.
805 *Continental Shelf Research*, *29*(8), 1053-1059. <https://doi.org/10.1016/j.csr.2008.11.016>
806
- 807 Deser, C., Alexander, M. A., Xie, S. P., & Phillips, A. S. (2010). Sea surface temperature
808 variability: Patterns and mechanisms. *Annual review of marine science*, *2*, 115-143.
809
- 810 Drouard, M., Kornhuber, K., & Woollings, T. (2019). Disentangling dynamic contributions to
811 summer 2018 anomalous weather over Europe. *Geophysical Research Letters*, *46*(21), 12537-
812 12546. <https://doi.org/10.1029/2019GL084601>
- 813 ECMWF (2022). Update on European heatwave of July 2022 (available at:
814 www.ecmwf.int/en/about/media-centre/focus/2022/update-european-heatwave-july-2022)
- 815 Faranda, D., Alvarez-Castro, M. C., Messori, G., Rodrigues, D., & Yiou, P. (2019). The
816 hammam effect or how a warm ocean enhances large scale atmospheric predictability. *Nature*
817 *communications*, *10*(1), 1-7. <https://doi.org/10.1038/s41467-019-09305-8>
- 818 Folland, C. K., Knight, J., Linderholm, H. W., Fereday, D., Ineson, S., & Hurrell, J. W.
819 (2009). The summer North Atlantic Oscillation: past, present, and future. *Journal of Climate*,
820 *22*(5), 1082-1103.

- 821 Fox-Kemper, B., H.T. Hewitt, C. Xiao, G. Aðalgeirsdóttir, S.S. Drijfhout, T.L. Edwards, N.R.
822 Golledge, M. Hemer, R.E. Kopp, G. Krinner, A. Mix, D. Notz, S. Nowicki, I.S. Nurhati, L.
823 Ruiz, J.-B. Sallée, A.B.A. Slangen, & Y. Yu, (2021). Ocean, Cryosphere and Sea Level
824 Change. In *Climate Change 2021: The Physical Science Basis. Contribution of Working*
825 *Group I to the Sixth Assessment Report of the Intergovernmental Panel on Climate Change*
826 [Masson-Delmotte, V., P. Zhai, A. Pirani, S.L. Connors, C. Péan, S. Berger, N. Caud, Y.
827 Chen, L. Goldfarb, M.I. Gomis, M. Huang, K. Leitzell, E. Lonnoy, J.B.R. Matthews, T.K.
828 Maycock, T. Waterfield, O. Yelekçi, R. Yu, and B. Zhou (eds.)]. Cambridge University Press,
829 Cambridge, United Kingdom and New York, NY, USA, 1211–1362. [https://doi.org/](https://doi.org/10.1017/9781009157896.011)
830 [10.1017/9781009157896.011](https://doi.org/10.1017/9781009157896.011)
831
- 832 Frölicher, T. L., Fischer, E. M., & Gruber, N. (2018). Marine heatwaves under global
833 warming. *Nature*, *560*(7718), 360-364. <https://doi.org/10.1038/s41586-018-0383-9>
- 834 Frölicher, T., & Laufkötter, C. (2018). Emerging risks from marine heat waves. *Nature*
835 *Communications*, *9*(1), 2015–2018. <https://doi.org/10.1038/s41467-018-03163-6>
- 836 Gómez, F., & Souissi, S. (2008). The impact of the 2003 summer heat wave and the 2005 late
837 cold wave on the phytoplankton in the north-eastern English Channel. *Comptes Rendus -*
838 *Biologies*, *331*(9), 678–685. <https://doi.org/10.1016/j.crv.2008.06.005>
- 839 Guinaldo, T., Voldoire, A., Waldman, R., Saux Picart, S., & Roquet, H. (2023). Response of
840 the sea surface temperature to heatwaves during the France 2022 meteorological summer.
841 *Ocean Science*, *19*(3), 629-647.
842
- 843 Guo, X., Gao, Y., Zhang, S., Wu, L., Chang, P., Cai, W., ... & Gao, H. (2022). Threat by
844 marine heatwaves to adaptive large marine ecosystems in an eddy-resolving model. *Nature*
845 *climate change*, *12*(2), 179-186.
846
- 847 Hersbach, H., Bell, B., Berrisford, P., Hirahara, S., Horányi, A., Muñoz-Sabater, J., ... &
848 Thépaut, J. N. (2020). The ERA5 global reanalysis. *Quarterly Journal of the Royal*
849 *Meteorological Society*, *146*(730), 1999-2049. (Accessed on 25-05-2023)
- 850 Hobday, A. J., Alexander, L. V., Perkins, S. E., Smale, D. A., Straub, S. C., Oliver, E. C. J.,
851 Benthuisen, J. A., Burrows, M. T., Donat, M. G., Feng, M., Holbrook, N. J., Moore, P. J.,
852 Scannell, H. A., Sen Gupta, A., & Wernberg, T. (2016). A hierarchical approach to defining
853 marine heatwaves. *Progress in Oceanography*, *141*, 227–238.
854 <https://doi.org/10.1016/j.pocean.2015.12.014>
855
- 856 Holbrook, N. J., Scannell, H. A., Sen Gupta, A., Benthuisen, J. A., Feng, M., Oliver, E. C.,
857 Alexander, L., Burrows, M., Donat, M., Hobday, A., Moore, P., Perkins-Kirkpatrick, S.,
858 Smale, D., Straub, S., & Wernberg, T. (2019). A global assessment of marine heatwaves and
859 their drivers. *Nature Communications*, *10*(1), 1-13. [https://doi.org/10.1038/s41467-019-](https://doi.org/10.1038/s41467-019-10206-z)
860 [10206-z](https://doi.org/10.1038/s41467-019-10206-z)
861

- 862 Huang, B., C. Liu, V. Banzon, E. Freeman, G. Graham, B. Hankins, T. Smith, and H.-M.
863 Zhang, 2020: Improvements of the Daily Optimum Interpolation Sea Surface Temperature
864 (DOISST) Version 2.1, *Journal of Climate*, 34, 2923-2939. [https://doi.org/10.1175/JCLI-D-](https://doi.org/10.1175/JCLI-D-20-0166)
865 20-0166
- 866 Hurrell, J. W., Kushnir, Y., Ottersen, G., & Visbeck, M. (2003). An overview of the North
867 Atlantic oscillation. *Geophysical Monograph-American Geophysical Union*, 134, 1-36.
868 <https://doi.org/10.1029/134GM01>
- 869 Izquierdo, P., Rico, J. M., Taboada, F. G., González-Gil, R., & Arrontes, J. (2022a).
870 Characterization of marine heatwaves in the Cantabrian Sea, SW Bay of Biscay. *Estuarine,
871 Coastal and Shelf Science*, 274(June). <https://doi.org/10.1016/j.ecss.2022.107923>
- 872 Izquierdo, P., Taboada, F. G., González-Gil, R., Arrontes, J., & Rico, J. M. (2022b).
873 Alongshore upwelling modulates the intensity of marine heatwaves in a temperate coastal sea.
874 *Science of the Total Environment*, 835(February).
875 <https://doi.org/10.1016/j.scitotenv.2022.155478>
- 876 Joint, I., & Smale, D. A. (2017). Marine heatwaves and optimal temperatures for microbial
877 assemblage activity. *FEMS Microbiology Ecology*, 93(2), 1–9.
878 <https://doi.org/10.1093/femsec/fiw243>
- 879 Josey, S.A., Hirschi, J.-M., Sinha, B., Duchez, A., Grist, J.P., Marsh, R., 2018. The recent
880 Atlantic cold anomaly: Causes, consequences, and related phenomena. *Ann. Rev. Marine Sci.*
881 10 (1), 475–501.
- 882 Kornhuber, K., Osprey, S., Coumou, D., Petri, S., Petoukhov, V., Rahmstorf, S., & Gray, L.
883 (2019). Extreme weather events in early summer 2018 connected by a recurrent hemispheric
884 wave-7 pattern. *Environmental Research Letters*, 14(5), 054002.
885 <https://doi.org/10.1088/1748-9326/ab13bf>
886
- 887 Le Boyer, A., Cambon, G., Daniault, N., Herbette, S., Le Cann, B., Marie, L., & Morin, P.
888 (2009). Observations of the Ushant tidal front in September 2007. *Continental Shelf Research*,
889 29(8), 1026-1037.
890
- 891 Lima, F. P., & Wetthey, D. S. (2012). Three decades of high-resolution coastal sea surface
892 temperatures reveal more than warming. *Nature communications*, 3(1), 704.
893
- 894 Lorenzo, M. N., Taboada, J. J., & Gimeno, L. (2008). Links between circulation weather
895 types and teleconnection patterns and their influence on precipitation patterns in Galicia (NW
896 Spain). *International Journal of Climatology: A Journal of the Royal Meteorological Society*,
897 28(11), 1493-1505. <https://doi.org/10.1002/joc.1646>
898

- 899 Marin, M., Feng, M., Phillips, H. E., & Bindoff, N. L. (2021). A global, multiproduct analysis
900 of coastal marine heatwaves: Distribution, characteristics, and long-term trends. *Journal of*
901 *Geophysical Research: Oceans*, 126(2), e2020JC016708.
902
- 903 McCarthy, M., Christidis, N., Dunstone, N., Fereday, D., Kay, G., Klein-Tank, A., Lowe, J.,
904 Petch, J., Scaife, A., & Stott, P. (2019). Drivers of the UK summer heatwave of 2018.
905 *Weather*, 74(11), 390-396. <https://doi.org/10.1002/wea.3628>
- 906 Met Office (2018). Summer 2018.
907 [https://www.metoffice.gov.uk/binaries/content/assets/metofficegovuk/pdf/weather/learn-](https://www.metoffice.gov.uk/binaries/content/assets/metofficegovuk/pdf/weather/learn-about/uk-past-events/interesting/2018/summer-2018---met-office.pdf)
908 [about/uk-past-events/interesting/2018/summer-2018---met-office.pdf](https://www.metoffice.gov.uk/binaries/content/assets/metofficegovuk/pdf/weather/learn-about/uk-past-events/interesting/2018/summer-2018---met-office.pdf)
- 909 Météo-France (2018). Bilan climatique de l'été 2018.
910 <https://meteofrance.fr/sites/meteofrance.fr/files/files/editorial/Bilan-climatique-annee2018.pdf>
911
- 912 Mieszkowska, N., Burrows, M., & Sugden, H. (2020). Impacts of climate change on intertidal
913 habitats, relevant to the coastal and marine environment around the UK. *MCCIP Science*
914 *Review 2020*, 256-271. <https://doi.org/10.14465/2020.arc12.ith>
- 915 Müller, H., Blanke, B., Dumas, F., & Mariette, V. (2010). Identification of typical scenarios
916 for the surface Lagrangian residual circulation in the Iroise Sea. *Journal of Geophysical*
917 *Research: Oceans*, 115(C7).
- 918 Norris, J., Vaughan, G., & Schultz, D. M. (2013). Snowbands over the English Channel and
919 Irish Sea during cold-air outbreaks. *Quarterly Journal of the Royal Meteorological Society*,
920 139(676), 1747-1761. <https://doi.org/10.1002/qj.2079>
- 921 Oh, H., Kim, G. U., Chu, J. E., Lee, K., & Jeong, J. Y. (2023). The record-breaking 2022
922 long-lasting marine heatwaves in the East China Sea. *Environmental Research Letters*, 18(6),
923 064015.
- 924 Oliver, E. C., Donat, M. G., Burrows, M. T., Moore, P. J., Smale, D. A., Alexander, L. V., ...
925 & Wernberg, T. (2018). Longer and more frequent marine heatwaves over the past century.
926 *Nature communications*, 9(1), 1-12.
- 927 Oliver, E. C. J., Burrows, M. T., Donat, M. G., Sen Gupta, A., Alexander, L. V., Perkins-
928 Kirkpatrick, S. E., Benthuisen, J. A., Hobday, A. J., Holbrook, N. J., Moore, P. J., Thomsen,
929 M. S., Wernberg, T., & Smale, D. A. (2019). Projected Marine Heatwaves in the 21st Century
930 and the Potential for Ecological Impact. *Frontiers in Marine Science*, 6(December), 1–12.
931 <https://doi.org/10.3389/fmars.2019.00734>
932
- 933 Plecha, S., & Soares, P. M. M. (2020) Global marine heatwave events using the new CMIP6
934 multi-model ensemble: from shortcomings in present climate to future projections,
935 *Environmental Research Letters*, 15 (12), 124058. <https://doi.org/10.1088/1748-9326/abc847>

- 936 Plecha, S. M., Soares, P. M. M., Silva-Fernandes, S. M., & Cabos, W. (2021). On the
937 uncertainty of future projections of Marine Heatwave events in the North Atlantic Ocean.
938 *Climate Dynamics*, 56, 2027–2056. <https://doi.org/10.1007/s00382-020-05529-3>
- 939 Poppeschi, C., Charria, G., Goberville, E., Rimmelin-Maury, P., Barrier, N., Petton, S.,
940 Unterberger, M., Grossteffan, E., Repecaud, M., Quemener, L., Theetten, S., Le Roux, J.-F. &
941 Tréguer, P. (2021). Unraveling salinity extreme events in coastal environments: A winter
942 focus on the bay of brest. *Frontiers in Marine Science*, 8, 705403.
943 <https://doi.org/10.3389/fmars.2021.705403>
944
- 945 Poppeschi, C., Charria, G., Daniel, A., Verney, R., Rimmelin-Maury, P., Retho, M.,
946 Goberville, E., Grossteffan, E., & Plus, M. (2022). Interannual variability of the initiation of
947 the phytoplankton growing period in two French coastal ecosystems. *Biogeosciences*, 19,
948 5667–5687. <https://doi.org/10.5194/bg-19-5667-2022>
949
- 950 Reynolds R W, Smith T M, Liu C, Chelton D B, Casey K Sand Schlab M G 2007 Daily high-
951 resolution-blended analyses for sea surface temperature, *J. Clim.* 20 5473–96
- 952 Ruthrof, K. X., Breshears, D. D., Fontaine, J. B., Froend, R. H., Matusick, G., Kala, J., Miller,
953 B. P., Mitchell, P. J., Wilson, S. K., van Keulen, M., Enright, N. J., Law, D. J., Wernberg, T.,
954 & Hardy, G. E. S. J. (2018). Subcontinental heat wave triggers terrestrial and marine, multi-
955 taxa responses. *Scientific Reports*, 8(1), 1–9. <https://doi.org/10.1038/s41598-018-31236-5>
- 956 Savu, A. (2022). Temperature Highs, Climate Change Salience, and Eco-Anxiety: Early
957 Evidence from the 2022 United Kingdom Heatwave. *Climate Change Salience, and Eco-*
958 *Anxiety*
- 959 Sims, D. W., Wearmouth, V. J., Genner, M. J., Southward, A. J., & Hawkins, S. J. (2004).
960 Low-temperature-driven early spawning migration of a temperate marine fish. *Journal of*
961 *Animal Ecology*, 73(2), 333-341.
- 962 Smale, D. A., Wernberg, T., Oliver, E. C. J., Thomsen, M., Harvey, B. P., Straub, S. C.,
963 Burrows, M. T., Alexander, L. V., Benthuyssen, J. A., Donat, M. G., Feng, M., Hobday, A. J.,
964 Holbrook, N. J., Perkins-Kirkpatrick, S. E., Scannell, H. A., Sen Gupta, A., Payne, B. L., &
965 Moore, P. J. (2019). Marine heatwaves threaten global biodiversity and the provision of
966 ecosystem services. *Nature Climate Change*, 9(4), 306–312. [https://doi.org/10.1038/s41558-](https://doi.org/10.1038/s41558-019-0412-1)
967 [019-0412-1](https://doi.org/10.1038/s41558-019-0412-1)
- 968 Seuront, L., Nicastro, K. R., Zardi, G. I., & Goberville, E. (2019). Decreased thermal
969 tolerance under recurrent heat stress conditions explains summer mass mortality of the blue
970 mussel *Mytilus edulis*. *Scientific Reports*, 9(1), 1–14. [https://doi.org/10.1038/s41598-019-](https://doi.org/10.1038/s41598-019-53580-w)
971 [53580-w](https://doi.org/10.1038/s41598-019-53580-w)
- 972 Schlegel R.W., E.C.J. Oliver, T. Wernberg, A.J. Smit (2017) Nearshore and offshore co-
973 occurrence of marine heatwaves and cold-spells, *Progress in Oceanography*, 151, 189-205.
974 <https://doi.org/10.1016/j.pocean.2017.01.004>

- 975 Schlegel, R. W., Darmaraki, S., Benthuyssen, J. A., Filbee-Dexter, K., Oliver, E. C. J. (2021)
976 Marine cold-spells, *Progress in Oceanography*, 198, 102684.
977 <https://doi.org/10.1016/j.pocean.2021.102684>
- 978 Simon, A., Plecha, S. M., Russo, A., Teles-Machado, A., Donat, M. G., Auger, P. A., &
979 Trigo, R. M. (2022). Hot and cold marine extreme events in the Mediterranean over the period
980 1982-2021. *Frontiers in Marine Science*, 9(August), 1–12.
981 <https://doi.org/10.3389/fmars.2022.892201>
- 982 Southward, A. J. (1960). On changes of sea temperature in the english channel. *Journal of the*
983 *Marine Biological Association of the United Kingdom*, 39(3), 449–458.
984 <https://doi.org/10.1017/S0025315400013473>
- 985 Wang, Y., Kajtar, J. B., Alexander, L. V., Pilo, G. S., & Holbrook, N. J. (2022).
986 Understanding the changing nature of marine cold-spells. *Geophysical Research Letters*, 49,
987 e2021GL097002. <https://doi.org/10.1029/2021GL097002>
- 988 Wethey, D. S., & Woodin, S. A. (2022). Climate change and *Arenicola marina*: Heat waves
989 and the southern limit of an ecosystem engineer. *Estuarine, Coastal and Shelf Science*,
990 276(December 2021), 108015. <https://doi.org/10.1016/j.ecss.2022.108015>
- 991 Wernberg, T., Bennett, S., Babcock, R. C., De Bettignies, T., Cure, K., Depczynski, M.,
992 Dufois, F., Fromont, J., Fulton, C. J., Hovey, R. K., Harvey, E. S., Holmes, T. H., Kendrick,
993 G. A., Radford, B., Santana-Garcon, J., Saunders, B. J., Smale, D. A., Thomsen, M. S.,
994 Tuckett, C. A., Tuya, F., Vanderklift, M. A., & Wilson, S. (2016). Climate-driven regime shift
995 of a temperate marine ecosystem. *Science*, 353(6295), 169–172.
996 <https://doi.org/10.1126/science.aad8745>
997
- 998 Vogel, M. M., Zscheischler, J., Wartenburger, R., Dee, D., & Seneviratne, S. I. (2019).
999 Concurrent 2018 hot extremes across Northern Hemisphere due to human-induced climate
1000 change. *Earth's future*, 7(7), 692-703. <https://doi.org/10.1029/2019EF001189>
1001
- 1002 Yao, Y., Wang, C., & Fu, Y. (2022). Global Marine Heatwaves and Cold-Spells in Present
1003 Climate to Future Projections. *Earth's Future*, 10(11), e2022EF002787.
1004
- 1005 Yiou, P., Cattiaux, J., Faranda, D., Kadygrov, N., Jézéquel, A., Naveau, P., Ribes, A., Robin,
1006 Y., Thao, S., Oldenborgh, G. J. & Vrac, M. (2020). Analyses of the Northern European
1007 summer heatwave of 2018. *Bulletin of the American Meteorological Society*, 101(1), S35-S40.
1008 <https://doi.org/10.1175/BAMS-D-19-0170.1ff>.